

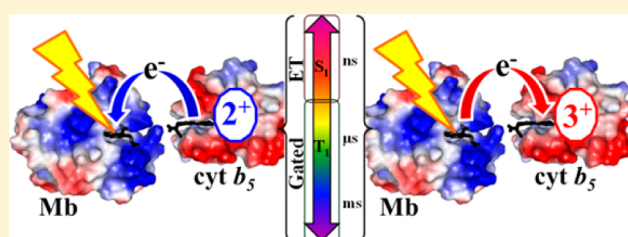
# Symmetrized Photoinitiated Electron Flow within the [Myoglobin:Cytochrome $b_5$ ] Complex on Singlet and Triplet Time Scales: Energetics vs Dynamics

Nadia Petlakh Co,<sup>†</sup> Ryan M. Young,<sup>†,‡</sup> Amanda L. Smeigh,<sup>†,‡</sup> Michael R. Wasielewski,<sup>†,‡</sup> and Brian M. Hoffman<sup>\*,†</sup>

<sup>†</sup>Department of Chemistry and <sup>‡</sup>Argonne-Northwestern Solar Energy Research (ANSER) Center, Northwestern University, Evanston, Illinois 60208-3113, United States

## S Supporting Information

**ABSTRACT:** We report here that photoinitiated electron flow involving a metal-substituted ( $M = \text{Mg, Zn}$ ) myoglobin (Mb) and its physiological partner protein, cytochrome  $b_5$  (cyt  $b_5$ ) can be “symmetrized”: the [Mb:cyt  $b_5$ ] complex stabilized by three D/E  $\rightarrow$  K mutations on Mb (D44K/D60K/E85K, denoted MMb) exhibits both oxidative and reductive ET quenching of both the singlet and triplet photoexcited MMb states, the direction of flow being determined by the oxidation state of the cyt  $b_5$  partner. The first-excited singlet state of MMb ( $^1\text{MMb}$ ) undergoes ns-time scale reductive ET quenching by  $\text{Fe}^{2+}\text{cyt } b_5$  as well as ns-time scale oxidative ET quenching by  $\text{Fe}^{3+}\text{cyt } b_5$ , both processes involving an ensemble of structures that do not interconvert on this time scale. Despite a large disparity in driving force favoring photooxidation of  $^1\text{MMb}$  relative to photoreduction ( $\delta(-\Delta G^0) \approx 0.4 \text{ eV}$ ,  $M = \text{Mg}$ ;  $\approx 0.2 \text{ eV}$ ,  $M = \text{Zn}$ ), for each  $M$  the average rate constants for the two reactions are the same within error,  $^1k_f > 10^8 \text{ s}^{-1}$ . This surprising observation is explained by considering the driving-force dependence of the Franck–Condon factor in the Marcus equation. The triplet state of the myoglobin ( $^3\text{MMb}$ ) created by intersystem crossing from  $^1\text{MMb}$  likewise undergoes reductive ET quenching by  $\text{Fe}^{2+}\text{cyt } b_5$  as well as oxidative ET quenching by  $\text{Fe}^{3+}\text{cyt } b_5$ . As with singlet ET, the rate constants for oxidative ET quenching and reductive ET quenching on the triplet time scale are the same within error,  $^3k_f \approx 10^5 \text{ s}^{-1}$ , but here the equivalence is attributable to gating by intracomplex conversion among a conformational ensemble.



## INTRODUCTION

Cytochrome  $b_5$  (cyt  $b_5$ ) reacts with myoglobin (Mb) as part of a physiological repair system in which autooxidized and inactive  $\text{Fe}^{3+}\text{Mb}$  is reduced to its active  $\text{Fe}^{2+}\text{Mb}$   $\text{O}_2$ -storage form by electron transfer (ET) from  $\text{Fe}^{2+}\text{cyt } b_5$ .<sup>1,2</sup> The [Mb:cyt  $b_5$ ] complex has served as a paradigm for interprotein ET between dynamically docked partners whose binding and reactivity are decoupled; many conformations of the complex contribute to binding but few to ET.<sup>3</sup> In recent years, we have demonstrated that binding and reactivity can be enhanced and coupled in the [Mb:cyt  $b_5$ ] complex through mutations on the MbWT surface and/or heme neutralization. These generate a suite of positively charged Mb's whose binding to the negatively charged  $b_5$  increases with the charge product of the proteins ( $-q_{\text{Mb}}q_{\text{cyt } b_5}$ );<sup>4,5</sup> ET between the Mb's and cyt  $b_5$  was probed through replacement of the heme group in Mb with a porphyrin containing a closed-shell metal ion ( $\text{Zn}^{2+}$ ), with the focus being photooxidation of the photoexcited triplet state,  $^3\text{ZnMb}$ . Most of this work studied  $^3\text{ZnMb}$  by  $\text{Fe}^{3+}\text{cyt } b_5$  on the time scale of milliseconds–seconds. However, photoexcitation of  $\text{ZnMb}$  directly populates the first-excited singlet state,  $S_1$ , and we discovered interprotein photooxidative singlet ET within a redesigned [ZnMb:cyt  $b_5$ ] complex at rate constants that

approach those occurring within the photosynthetic reaction centers,  $k_{\text{ET}} = 2.1 \times 10^9 \text{ s}^{-1}$ .<sup>6</sup>

In the rich history of photoinitiated interprotein ET where one partner is a metal-substituted hemoprotein ( $M = \text{H}_2$  as well as  $\text{Mg, Zn}$ ), the exclusive focus has been on oxidative ET quenching of the photoexcited protein partner,<sup>7–15</sup> despite the fact that photoreduction of  $M$ -porphyrins is energetically favorable,<sup>16,17</sup> and that there have been reports of reductive and oxidative quenching of photoexcited  $\text{Zn}$ -substituted proteins by small molecules.<sup>18,19</sup> We report here that photoinitiated electron flow involving a metal-substituted hemoprotein and its physiological partner protein can indeed be “symmetrized”: the [Mb:cyt  $b_5$ ] complex stabilized by three D/E  $\rightarrow$  K mutations on Mb (MMb(D44K/D60K/E85K), denoted MMb;  $M = \text{Mg}$  or  $\text{Zn}$ ) exhibits both oxidative and reductive ET quenching of both the singlet and triplet photoexcited MMb states, the direction of flow being determined by the oxidation state of the cyt  $b_5$  partner. We find that the first-excited singlet state,  $S_1$ , of the Mb-incorporated metalloporphyrin, denoted  $^1\text{MMb}$ , undergoes nanosecond-time scale reductive ET

Received: June 25, 2014

Published: August 18, 2014

quenching in which an electron is transferred to  $^1\text{MMb}$  from  $\text{Fe}^{2+}\text{cyt } b_5$ , as well as nanosecond-time scale oxidative ET quenching in which an electron is transferred from  $^1\text{MMb}$  to  $\text{Fe}^{3+}\text{cyt } b_5$ . Surprisingly, the rate constants for the two intracomplex reactions are the same within error, with average rate constants,  $^1k_f \approx 10^8 \text{ s}^{-1}$ , a phenomenon that is explainable on energetic grounds. The progress curves in both cases are nonexponential and viscosity independent, implying the presence of ensembles of structures that do not interconvert on the time scale of the measurement.

The triplet state of the mutant,  $^3\text{MMb}$ , created by intersystem crossing (ISC) from  $^1\text{MMb}$  likewise undergoes reductive ET quenching by the  $\text{Fe}^{2+}\text{cyt } b_5$  as well as oxidative ET quenching by the  $\text{Fe}^{3+}\text{cyt } b_5$ . Again, surprisingly, the rate constants for the two intracomplex reactions are the same within error,  $^3k_f \approx 10^5 \text{ s}^{-1}$ , despite a large disparity in driving forces. However, in this case the shape and viscosity dependence of the progress curves indicate that ET is gated by intracomplex conversion among a conformational ensemble.

## MATERIALS AND METHODS

The protocols for expression, reconstitution with the desired metalloporphyrin, M (M is Mg-protoporphyrin IX = Mg or Zn-deuteroporphyrin IX = Zn), and purification of Mb(D44K/D60K/E85K) have been outlined elsewhere,<sup>4,5</sup> and are briefly described in the Expanded Materials and Methods section in Supporting Information (SI). The tryptic fragment of bovine cyt  $b_5$  was isolated and purified as described previously.<sup>20,21</sup> Aerobic cyt  $b_5$  prefers the ferric state because of its slight negative redox potential ( $-0.006 \text{ V}$  vs NHE).<sup>22</sup> However, for oxidative quenching experiments in which cyt  $b_5$  served as the oxidizing agent, it was further treated with excess  $\text{K}_3[\text{Fe}(\text{CN})_6]$  and then washed thoroughly with working buffer (5 mM KPi, pH 6). For reductive quenching experiments in which cyt  $b_5$  served as the reducing agent, it was treated with excess  $\text{Na}_2\text{S}_2\text{O}_4$  and then washed thoroughly with working buffer.

Samples were prepared in a COY anaerobic glovebox. The working buffer (5 mM KPi, pH 6.0 or 70% w/w glycerol in 5 mM KPi, pH 6) was syringe-filtered and allowed to deoxygenate in the glovebox for at least 24 h before the samples were made. Protein stock solutions were exchanged into the anaerobic working buffer using Corning Spin-X UF concentrators immediately prior to the measurements. Three types of sample were prepared: MMb by itself, cyt  $b_5$  by itself, and the complex,  $[\text{MMb}:\text{cyt } b_5]$ . The details concerning sample volumes and concentrations for femtosecond- and nanosecond-transient absorption (TA) can be found in SI.

Singlet quenching was measured via fs-TA.<sup>23</sup> The  $\sim 120 \text{ fs}$  pulses were produced with a commercial Ti:sapphire oscillator/amplifier (Tsunami/Spitfire, Spectra-Physics), generating  $\sim 1 \text{ W}$  at 827 nm, operating at 1 kHz. About 40% of this output was frequency-doubled and directed to a two-stage OPA producing pulses of 540 nm (ZnMb samples) or 598 nm (MgMb samples). Five percent of the amplified pulse was sent up and down a motorized delay track which provided the desired time resolution, then was focused onto a sapphire disk to create a white-light continuum probe with coverage from 430 to 850 nm. After passing through the sample, the probe beam was dispersed onto a CMOS array detector for the collection of spectral data at multiple delay times following photoexcitation of the sample. Samples were stirred to reduce the effects of photodegradation and local heating. Transient absorption spectra were obtained by chopping the pump beam at 500 Hz and subtracting pump-on versus pump-off spectra. Data were treated with a group-delay dispersion correction prior to analysis. Progress curves were generated at multiple wavelengths from the TA spectra and fit using an exponential (for  $^1\text{MMb}$  decay) or a stretched exponential<sup>24</sup> (for  $^1\text{MMb}$  reaction with cyt  $b_5$ ) (see Results and Discussion). Additional experimental and data analysis details are available in SI.

Triplet quenching was measured via ns-TA. Samples were excited with a Nd:YAG Quanta-Ray INDI laser (Spectra-Physics) tuned to

532 nm.<sup>6</sup> The output power was set to approximately 20 mW for the MgMb samples. Triplet measurements were performed with an LKS.60 laser flash photolysis spectrometer (Applied Photophysics) fitted with a xenon lamp with pulsing capabilities as the probe source. The submicrosecond–millisecond collection mode uses an Agilent Infinium 600 MHz digitizer with a five-stage 1P28 photomultiplier tube as the detector. The xenon lamp was pulsed for submicrosecond collections. The triplet decay time courses were monitored at 465 nm, the maxima for the triplet-ground spectra difference for these samples. All kinetic experiments were performed at 20 °C. As decay traces span several orders of magnitude in time, 50–100 shots were averaged for each time-segment and then merged into single files to obtain full kinetic progress curves for analysis.

## RESULTS AND DISCUSSION

### Energetics of ET between $^1\text{MMb}/^3\text{MMb}$ and cyt $b_5$ .

The driving forces ( $-\Delta G^0$ ) for the charge separation reactions generated by the photoinitiated oxidation or reduction of  $^1\text{MgMb}$  by ferric cyt  $b_5$  or ferrous cyt  $b_5$ , calculated as described in SI, are presented within the ET cycle of Scheme 1 and in Table 1. The driving forces for charge recombination follow

Scheme 1

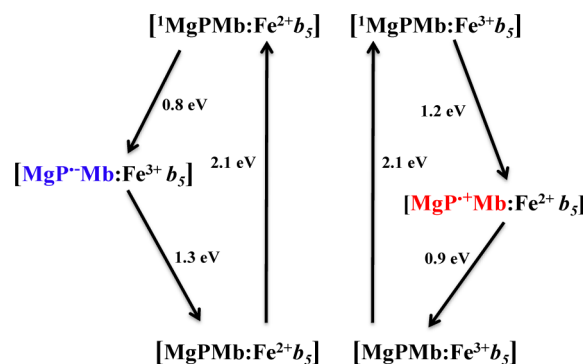


Table 1. Driving Forces ( $-\Delta G^0$ ) for the Singlet and Triplet ET Charge Separation and Recombination Reactions for the  $[\text{MgMb}:\text{Fe}^{3+}\text{cyt } b_5]$  and  $[\text{MgMb}:\text{Fe}^{2+}\text{cyt } b_5]$  Complexes

		charge separation, $-\Delta G^0$ (eV)	charge recombination, $-\Delta G^0$ (eV)
singlet ET	$[\text{MgMb}:\text{Fe}^{3+}\text{cyt } b_5]$	1.2	0.9
	$[\text{MgMb}:\text{Fe}^{2+}\text{cyt } b_5]$	0.8	1.3
triplet ET	$[\text{MgMb}:\text{Fe}^{3+}\text{cyt } b_5]$	0.8	0.9
	$[\text{MgMb}:\text{Fe}^{2+}\text{cyt } b_5]$	0.4	1.3

from closing the thermodynamic cycle and are also given in Scheme 1 and Table 1. Both oxidative and reductive ET quenching of  $^1\text{MgMb}$  by  $\text{Fe}^{3+}\text{cyt } b_5$  (right side of Scheme 1) and  $\text{Fe}^{2+}\text{cyt } b_5$  (left side of Scheme 1), respectively, are seen to be strongly energetically favorable ( $-\Delta G^0 \gg 0$ ). The photoinitiated oxidation or reduction charge separation reactions of  $^1\text{ZnMb}$  by ferric or ferrous cyt  $b_5$  are comparably energetically favorable (Scheme S1 in SI).

The corresponding driving forces ( $-\Delta G^0$ ) for  $^3\text{MgMb}$  oxidation or reduction charge separation reactions with ferric or ferrous cyt  $b_5$  were calculated analogously; again, both oxidative and reductive ET quenching of  $^3\text{MgMb}$  by cyt  $b_5$  are highly favorable (Table 1; Scheme S2 in SI).

**Singlet State ( $^1\text{MMb}$ ) Electron Transfer Quenching.** MgMb forms 1:1 cyt  $b_5$  complexes with dissociation constant,

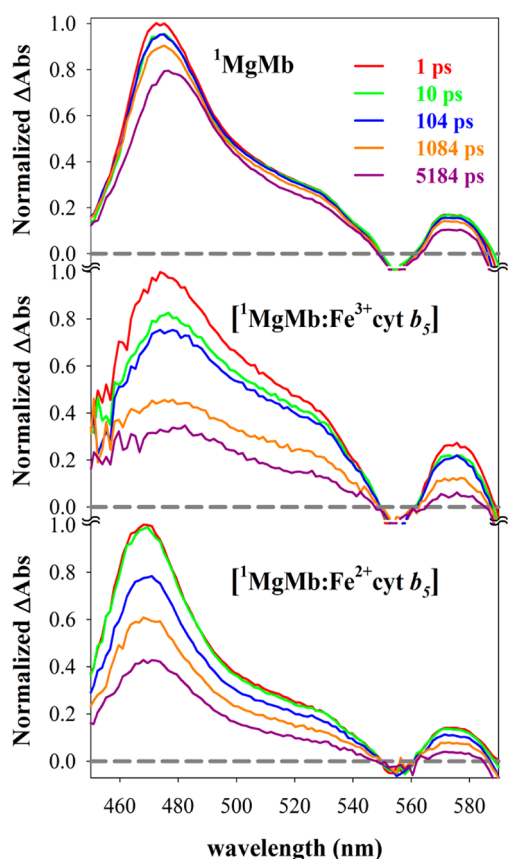


**Figure 1.** Difference spectra for  $^1\text{MgMb}$  by itself (top), in complex with  $\text{Fe}^{3+}\text{cyt } b_5$  (middle), and in complex with  $\text{Fe}^{2+}\text{cyt } b_5$  (bottom).

$K_d \approx 10 \mu\text{M}$ , as does  $\text{ZnMb}$ .<sup>6</sup> Figure 1 displays the absorbance-difference spectra in the 450–600 nm region, collected subsequent to laser excitation over the time scale of  $S_1$  decay for (i)  $\text{MgMb}$  by itself (top panel, Figure 1) and for complexes with (ii)  $\text{Fe}^{3+}\text{cyt } b_5$  (middle, Figure 1) and (iii)  $\text{Fe}^{2+}\text{cyt } b_5$  (bottom, Figure 1); the concentrations of  $\text{cyt } b_5$  were chosen so that  $\geq 90\%$  of the  $\text{MMb}$  was in complex. As can be seen, the singlet-ground absorbance-difference spectra at  $t = 1$  ps for the free  $\text{MgMb}$  and for the two complexes are essentially the same; the same is true for  $\text{ZnMb}$  (Figure S1 in SI). The traces of Figure 1 show the  $^1\text{MgMb}$  difference spectrum collected out to 5.2 ns; the absorbance difference persisting after this time is due to the triplet-ground difference generated by  $^1\text{MgMb}$  that undergo ISC to  $^3\text{MgMb}$ , which does not decay on the ns singlet time scale.

As clearly seen in Figure 1, the  $^1\text{MgMb}$  excited state is strongly quenched by complex formation with the  $\text{cyt } b_5$  partner protein in both its  $\text{Fe}^{3+}$  and  $\text{Fe}^{2+}$  oxidation states. Analogous behavior is observed for  $^1\text{ZnMb}$  (Figure S1 in SI), but  $^1\text{MgMb}$  decays approximately 5 times more slowly than  $^1\text{ZnMb}$ , allowing for relatively clearer characterization of  $^1\text{MgMb}$  ET quenching, and consequently, we focus on this variant here. The progress curves for the decay of  $^1\text{MgMb}$ , both free and in the two complexes were assembled from the absorbance-difference spectra slices at 465 nm and are shown in Figure 2. See Figure S2 in SI for progress curves of free  $^1\text{ZnMb}$  and in complex with  $\text{Fe}^{3+}\text{cyt } b_5$  and  $\text{Fe}^{2+}\text{cyt } b_5$ . The free  $^1\text{MMb}$  ( $M = \text{Mg, Zn}$ ) decays exponentially (eq 1),

$$\Delta A = A_0 \exp(-^1k_D t) + C \quad (1)$$

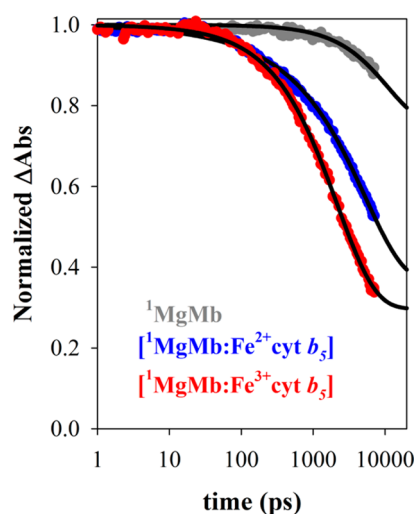


**Figure 2.** Progress curves for singlet to ground decay for  $^1\text{MgMb}$  (gray), reductive quenching of  $^1\text{MgMb}$  in the presence of  $\text{Fe}^{2+}\text{cyt } b_5$  (blue), and oxidative quenching of  $^1\text{MgMb}$  in the presence of  $\text{Fe}^{3+}\text{cyt } b_5$  (red). The  $^1\text{MgMb}$  trace is described by eq 1, while the  $[\text{MgMb}:\text{Fe}^{3+}\text{cyt } b_5]$  and  $[\text{MgMb}:\text{Fe}^{2+}\text{cyt } b_5]$  traces are best described by eq 2.

where  $A_0$  is the singlet-ground absorbance difference,  $^1k_D$  is the singlet decay constant, and  $C$  is the absorbance difference associated with the triplet state, which does not decay measurably on this time scale. Table 2 presents the derived  $^1k_D$ 's.

For both the  $[\text{MMb}:\text{Fe}^{3+}\text{cyt } b_5]$  and  $[\text{MMb}:\text{Fe}^{2+}\text{cyt } b_5]$  complexes, the strong quenching of  $^1\text{MMb}$  by the  $\text{cyt } b_5$  (Figure 1, Figure S1 in SI) generates rapidly decaying progress curves (Figure 2, Figure S2 in SI) that are well described by augmenting the intrinsic decay with a stretched exponential (eq 2).

$$\Delta A = A_0 \exp[-^1k_D t - (^1k_f t)^n] + C \quad (2)$$

This formulation describes an ensemble of complexes that exhibit a distribution in quenching constants around an average value,  $^1k_f$ , the breadth of the distribution is reflected in the distribution exponent,  $0 < n \leq 1$ , with smaller values for  $n$  corresponding to greater breadth of the distribution.<sup>24</sup>

The quenching constants for both  $^1\text{MMb}$ 's obtained by globally fitting the progress curves of Figures 2 and S2 in SI at multiple wavelengths to eq 2 are presented in Table 2; we note that the quenching constants for  $^1\text{ZnMb}$  are less reliably obtained because of the more rapid singlet decay. Given the high driving forces for both oxidative and reductive ET (Table 1 and Scheme 1) we attribute the  $S_1$  quenching in both  $[\text{MgMb}:\text{cyt } b_5]$  complexes to intracomplex ET: to photo-oxidation of the strongly reducing singlet excited state of  $\text{MgMb}$  through  $^1\text{MgMb} \rightarrow \text{Fe}^{3+}\text{cyt } b_5$  ET (Scheme 1, right-side of the photocycle) with the rate constant of  $^1k_{f,\text{ox}}$ ; to photoreduction of the  $S_1$  state by  $\text{Fe}^{2+}\text{cyt } b_5 \rightarrow ^1\text{MgMb}$  ET (Scheme 1, left-side of the photocycle) with the rate constant of  $^1k_{f,\text{red}}$ . Likewise, the  $S_1$  quenching in  $\text{ZnMb}$  complexes is attributed to intracomplex ET due to photooxidation or photoreduction with  $\text{Fe}^{3+}\text{cyt } b_5$  or  $\text{Fe}^{2+}\text{cyt } b_5$ , respectively (SI). As confirmation, analysis presented in SI demonstrates that resonance energy transfer from the excited  $^1\text{MgMb}/^1\text{ZnMb}$  to  $\text{Fe}^{3+}$  or  $\text{Fe}^{2+}\text{cyt } b_5$  cannot be a significant component of the quenching.

Efforts to measure the rate constant for charge recombination of the charge separated intermediates generated by ET between  $^1\text{MgMb}/^1\text{ZnMb}$  and  $\text{cyt } b_5$  were not successful. Such



Table 2. Fit Parameters for <sup>1</sup>MMb (M = Mg, Zn) Decay and Singlet ET with cyt b<sub>5</sub>

	[ <sup>1</sup> MgMb:Fe <sup>2+</sup> cyt b <sub>5</sub> ]	[ <sup>1</sup> MgMb:Fe <sup>3+</sup> cyt b <sub>5</sub> ]	[ <sup>1</sup> ZnMb:Fe <sup>2+</sup> cyt b <sub>5</sub> ]	[ <sup>1</sup> ZnMb:Fe <sup>3+</sup> cyt b <sub>5</sub> ]
<sup>1</sup> k <sub>D</sub> (s <sup>-1</sup> )	9.1(1) × 10 <sup>7</sup>		4.7(5) × 10 <sup>8</sup>	
<sup>1</sup> k <sub>f</sub> (s <sup>-1</sup> ), (n)	2.8(2) × 10 <sup>8</sup> (n = 0.50)	3.6(2) × 10 <sup>8</sup> (n = 0.74)	2.0(1) × 10 <sup>8</sup> (n = 0.50) <sup>a</sup>	2.9(8) × 10 <sup>8</sup> (n = 0.78)

<sup>a</sup>Due to less cleanly resolved quenching in the ZnMb complexes, the distribution exponent was fixed in eq 2 for [<sup>1</sup>ZnMb:Fe<sup>2+</sup>cyt b<sub>5</sub>] to the value obtained from fits to the [<sup>1</sup>MgMb:Fe<sup>2+</sup>cyt b<sub>5</sub>] progress curves.

measurements were carried out in an earlier study of photooxidation of a more tightly bound <sup>1</sup>MMb variant,<sup>6</sup> but that study showed that the charge recombination (back ET) reactions are faster than the charge separation (or forward ET) reactions, suppressing accumulation of the intermediate on the singlet time scale as well as the triplet time scale as discussed below. In the present study, this obstacle was compounded by the fact that in the wavelength range monitored (450–750 nm) there is no singlet/ground isosbestic point that could be used to optimally detect and monitor the intermediate, and the absorbance-difference for the charge-separated species is small relative to the singlet-ground absorbance difference throughout the range.

Surprisingly, the average rate constants for the photooxidation and photoreduction of <sup>1</sup>MgMb, respectively within the complexes with Fe<sup>3+</sup>cyt b<sub>5</sub> and Fe<sup>2+</sup>cyt b<sub>5</sub>, are roughly equal, <sup>1</sup>k<sub>f,ox</sub> ≈ <sup>1</sup>k<sub>f,red</sub>, despite the fact that the driving forces for the two charge separation processes differ by 0.4 eV (Table 1). Likewise, the average photooxidation and photoreduction rate constants of <sup>1</sup>ZnMb are also similar (Table 2). In short, the average ET quenching rate constant appears surprisingly insensitive to the direction of the electron flow—being essentially the same when <sup>1</sup>MMb is oxidized by Fe<sup>3+</sup>cyt b<sub>5</sub> or reduced by Fe<sup>2+</sup>cyt b<sub>5</sub>—and <sup>1</sup>k<sub>f</sub> is further insensitive to the identity of M (Table 2).

The fits of the ET quenching to a stretched exponential with *n* < 1 imply the presence of an ensemble of complexes with a distribution of singlet ET rate constants. Brownian Dynamics (BD) simulations, indeed predict the presence of such an ensemble, with M–Fe distances that range from 15 to 20 Å and a shortest reactivity distance of 15.3 Å for the complexes between the Mb mutant and cyt b<sub>5</sub>.<sup>25</sup> However, the observation of a distribution of quenching constants, rather than an average over the rate constants of the ensemble, further implies that the ensemble of bound complexes do not undergo conformational interconversion on the ET time scale. To test this implication, ET was measured for the [<sup>1</sup>MgMb:Fe<sup>3+</sup>cyt b<sub>5</sub>] and [<sup>1</sup>MgMb:Fe<sup>2+</sup>cyt b<sub>5</sub>] complexes in 70% w/w glycerol buffer, where the viscosity is ~20× greater than that of aqueous buffer. Figure 3 shows that the singlet kinetic data collected in glycerol and aqueous buffers overlay well for both oxidative and reductive quenching, and ET kinetic parameters for the two solvents differ insignificantly, confirming the absence of any role for conformational interconversion within the ensemble of structures during the nanosecond duration of the singlet ET charge separation process.

**Comparison of Oxidative and Reductive Singlet Electron Transfer.** We now show that, when the ET energetics for oxidation and reduction charge separation processes (Table 1) are incorporated in the Marcus equation, they fully account for the unexpectedly similar rate constants for the photooxidation and photoreduction of <sup>1</sup>MMb within the complexes with Fe<sup>3+</sup>cyt b<sub>5</sub> and Fe<sup>2+</sup>cyt b<sub>5</sub>, respectively. Marcus showed that an ET rate constant can be written as the product of two terms—the tunneling matrix element (*H*<sub>DA</sub><sup>2</sup>) and the Franck–Condon factor (*FC*). The former is a joint function of

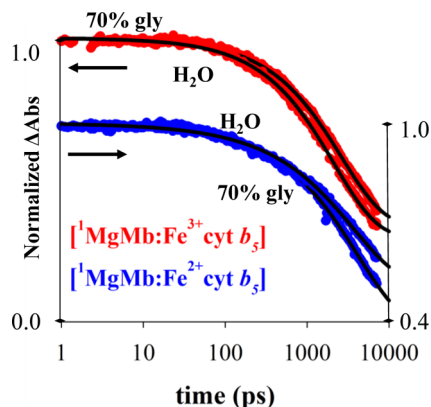


Figure 3. Progress curves for oxidative (red) and reductive (blue, offset by −0.3 arbitrary absorbance units) quenching of <sup>1</sup>MgMb by Fe<sup>3+</sup> and Fe<sup>2+</sup>cyt b<sub>5</sub>, respectively in 70% gly and aqueous buffer.

the distance between the donor and acceptor and the electron-transfer pathways (dictated by the protein as the intervening medium in this case), while the latter is a function of the driving force (−Δ*G*<sup>0</sup>) for the electron transfer reaction, eqs 3,

$$k_{\text{ET}} = \frac{2\pi}{\hbar} H_{\text{DA}}^2 \cdot FC \quad (3a)$$

$$FC = \frac{1}{\sqrt{4\pi\lambda k_{\text{B}}T}} \exp\left(\frac{-[\Delta G^0 + \lambda]^2}{4\lambda k_{\text{B}}T}\right) \quad (3b)$$

*FC* (eq 3b) is a “simple” parabolic function of the driving force (−Δ*G*<sup>0</sup>) for ET with maximum at −Δ*G*<sup>0</sup> = λ (where λ is the reorganization energy). Figure 4 plots *FC* as a function of −Δ*G*<sup>0</sup> for λ ≈ 1 eV;<sup>25</sup> previous reports have demonstrated that the same λ value is applicable to both oxidative and reductive charge recombination reactions for the same photoexcitable species.<sup>19</sup>

While the [<sup>1</sup>MgMb:Fe<sup>3+</sup>cyt b<sub>5</sub>] and [<sup>1</sup>MgMb:Fe<sup>2+</sup>cyt b<sub>5</sub>] complexes are expected to exhibit a similar ensemble of structures and electron-transfer pathways (due to the same ranges of reactivity distances and the same protein media) and, therefore, comparable *H*<sub>DA</sub><sup>2</sup>, the driving forces for the oxidative and reductive <sup>1</sup>MgMb ET charge separation processes differ by δ(−Δ*G*<sup>0</sup>) ≈ 0.4 eV (Table 1). However, Figure 4 highlights the unexpected fact that the two driving forces (depicted by circles) are symmetrically placed around and near the maximum of the parabola at −Δ*G*<sup>0</sup> = λ, oxidation being in the “inverted” region, −Δ*G*<sup>0</sup> > λ, reduction in the “normal” region, −Δ*G*<sup>0</sup> < λ. As a result, *FC* for the two processes is fortuitously the same. Moreover, since the two driving force values fall near the *FC* maximum, slight adjustments of either the −Δ*G*<sup>0</sup>s or λ would likely result in the same set of kinetic observations. Thus, the apparently surprising similarities in the <sup>1</sup>k<sub>f</sub> for the oxidative and reductive quenching of <sup>1</sup>MgMb are understandable on simple energetic grounds.

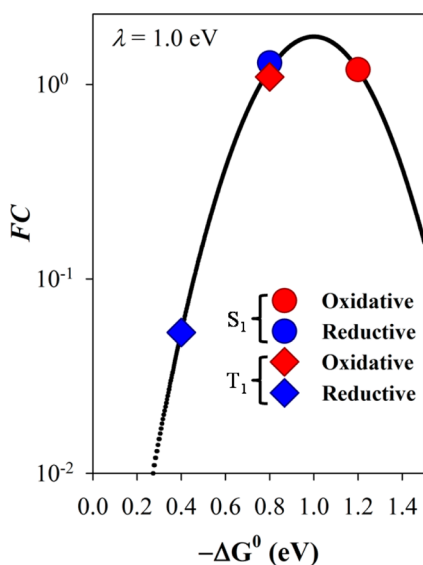


**Figure 4.** FC term as a function of driving forces ( $-\Delta G^0$ ) and  $\lambda = 1.0$  eV for ET in the MgMb complexes with cyt  $b_5$ . Singlet ET is represented by circles, and triplet ET, by diamonds. Oxidative quenching or ET from  $^1\text{MgMb}$  to  $\text{Fe}^{3+}\text{cyt } b_5$  is in red and reductive quenching or ET from  $\text{Fe}^{2+}\text{cyt } b_5$  to  $^1\text{MgMb}$  is in blue. Since  $-\Delta G^0 = 0.8$  eV (see Table 1) for reductive quenching due to singlet ET and oxidative quenching due to triplet ET, the FC terms for these two processes are offset by 0.1 in opposite directions for clarity.

Likewise,  $-\Delta G^0$ 's for singlet ET charge separation processes in the  $[\text{ZnMb}:\text{Fe}^{3+}\text{cyt } b_5]$  and  $[\text{ZnMb}:\text{Fe}^{2+}\text{cyt } b_5]$  complexes are symmetrically related to  $\lambda$  (Figure S4 in SI), again explaining why the oxidative and reductive singlet ET quenching reactions have similar  $^1k_i$ 's (Table 2). Additionally, the respective oxidative and reductive ET charge separation processes for the  $[\text{ZnMb}:\text{cyt } b_5]$  complexes have driving forces that are within  $\delta(-\Delta G^0) \approx 0.1$  eV (Scheme S1 in SI) of those for the  $[\text{MgMb}:\text{cyt } b_5]$  complexes (Scheme 1; Table 1), accounting for the M-independence of ET rate constants.

Examination of the parameter characterizing the breadth of the distribution in structures ( $n$ , eq 2) does, however, reveal a slight oversimplification in the above comments about  $H_{\text{DA}}^2$ . For both  $M = \text{Mg}$  and  $\text{Zn}$ , the distribution parameter for oxidative singlet ET quenching ( $n \approx 0.75$ ) appears to be meaningfully different than that for reductive singlet ET quenching ( $n \approx 0.50$ ) suggesting a broadening of the distribution of rate constants for reductive quenching in the complex,  $[\text{MgMb}:\text{Fe}^{2+}\text{cyt } b_5]$ , relative to oxidative quenching in the complex,  $[\text{MgMb}:\text{Fe}^{3+}\text{cyt } b_5]$  (Table 2). This dissimilarity can be attributed to a subtle variance in the ensemble of binding geometries resulting from the difference by a single charge in the two oxidation states, ferrous and ferric, of the highly negative cyt  $b_5$  partner in the two types of complexes.

**Oxidative and Reductive Electron Transfer in  $[\text{MgMb}:\text{cyt } b_5]$  Complexes.** Conformations of the  $[\text{MgMb}:\text{cyt } b_5]$  complexes that do not react via singlet ET (or relax to ground) instead undergo ISC to the  $[\text{MgMb}:\text{cyt } b_5]$  state, which can react via photooxidation or photoreduction of  $^3\text{MgMb}$  by the  $\text{Fe}^{3+}\text{cyt } b_5$  and  $\text{Fe}^{2+}\text{cyt } b_5$ , respectively, on the much longer (ms) triplet-state time scale. Figure 5 presents progress curves for triplet decay monitored at 465 nm, the maximum triplet-ground difference absorption wavelength, for samples of the  $[\text{MgMb}:\text{Fe}^{3+}\text{cyt } b_5]$  complex and the

$[\text{MgMb}:\text{Fe}^{2+}\text{cyt } b_5]$  complex in aqueous and 70% w/w glycerol buffers; in both cases  $\sim 80\%$  of the MgMb was in complex.

In the absence of cyt  $b_5$ ,  $^3\text{MgMb}$  decays to the ground state with first-order rate constant,  $^3k_D = 400 \text{ s}^{-1}$  independent of solvent (Figure 5). As previously reported, the  $[\text{Mb}:\text{cyt } b_5]$  complex is in the slow-exchange regime on the triplet ET time scale where ET is significantly faster than dissociation of the

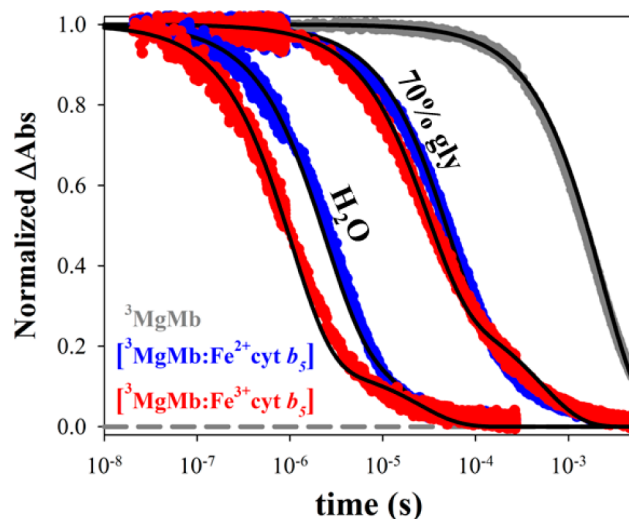


**Figure 5.** Triplet progress curves monitored at 465 nm: MgMb by itself in the absence of cyt  $b_5$  quencher in gray; in the presence of  $\text{Fe}^{2+}\text{cyt } b_5$  in blue; in the presence of  $\text{Fe}^{3+}\text{cyt } b_5$  in red. Triplet ET slows down with increased viscosity as noted by the rightward shift (toward  $^3k_D$ ) of the progress curves in 70% gly relative to the ones in aqueous buffer.

complex,  $^3k_{\text{ET}} \gg k_{\text{off}}$ .<sup>6</sup> As a result, triplet decay traces for the complex are biphasic (Figure 5) and can be fit to a double exponential (eqs 4): the rapidly decaying majority phase corresponds to the  $[\text{MgMb}:\text{cyt } b_5]$  complex (fraction  $R$ ), which decays with rate constant,  $^3k_{\text{obs},f} = ^3k_D + ^3k_f$  where  $^3k_f$  is the intracomplex triplet ET rate constant; the minority phase represents free  $^3\text{MgMb}$ , which undergoes slower bimolecular quenching ( $^3k_2$ ) with pseudo-first-order rate constant  $^3k_{\text{obs},s} = ^3k_D + ^3k_2[\text{cyt } b_5]$ .

$$\Delta A = A_0[R \cdot \exp(-^3k_{\text{obs},f}t) + (1 - R) \cdot \exp(-^3k_{\text{obs},s}t)] \quad (4a)$$

where

$$^3k_{\text{obs},f} = ^3k_D + ^3k_f; \quad ^3k_{\text{obs},s} = ^3k_D + ^3k_2[\text{cyt } b_5] \quad (4b)$$

The kinetic parameters resulting from fits to eqs 4 are listed in Table 3. Monitoring the triplet/ground isosbestic points yielded no quantifiable charge-separated intermediate signals for either the oxidative or reductive quenching charge separation triplet ET reactions, supporting the expectation that the accumulations of the respective charge-separated species are even smaller on the triplet time scale relative to the singlet time scale due to the relative lifetimes of the charge separation and charge recombination processes.<sup>26</sup>

The rate constants for intracomplex triplet ET,  $^3k_f$ 's, are essentially the same for the oxidative and reductive processes in the same type of solvent (Table 3), but in this case the identity is not in agreement with predictions of the Marcus theory based on the energetics for triplet ET quenching. As with

Table 3.  $^3k_f$ 's ( $s^{-1}$ ) and  $^3k_2$ 's ( $mM^{-1} s^{-1}$ ) for  $^3MgMb$  Reductive and Oxidative Quenching in Water and 70% w/w Glycerol

	$^3k_f$ ( $s^{-1}$ ), R		$^3k_2$ ( $mM^{-1} s^{-1}$ )	
	water, 1.005 cP (20 °C)	70% w/w gly, 22.5 cP (20 °C)	water, 1.005 cP (20 °C)	70% w/w gly, 22.5 cP (20 °C)
$[^3MgMb:Fe^{3+}cyt\ b_5]$	$9.7(1) \times 10^5$ , 0.85	$3.3(5) \times 10^4$ , 0.71	$8.1(2) \times 10^5$	$3.1(6) \times 10^4$
$[^3MgMb:Fe^{2+}cyt\ b_5]$	$4.3(6) \times 10^5$ , 0.77	$1.9(3) \times 10^4$ , 0.79	$1.1(2) \times 10^6$	$2.4(4) \times 10^4$

singlet ET, triplet ET is energetically favorable for both oxidative quenching ( $-\Delta G^0 = 0.8$  eV) and reductive quenching ( $-\Delta G^0 = 0.4$  eV) of the  $^3MgMb$  with the difference between these two driving forces also being  $\sim 0.4$  eV (Table 1). At the same time, the relative driving forces ( $-\Delta G^0$ ) are not symmetrically positioned around the estimated  $\lambda$  (Figure 4), and the FC, and  $^3k_{ET}$  is predicted to differ by more than an order of magnitude for the two charge separation processes:  $^3k_{ET,ox} > ^3k_{ET,red}$ .

The similarity of the two  $^3k_f$ 's instead are explained by comparing the progress curves for the complexes in aqueous ( $\eta \approx 1$ ) and 70% w/w glycerol buffers ( $\eta \approx 20$ ). As expected, the diffusion-limited second-order process slows in 70% w/w gly relative to water for both the photooxidative and photo-reductive reactions with  $^3k_2$  decreasing by a factor of  $\gtrsim 20$  as the viscosity increases by about this factor (Table 3). Unexpectedly, the rate constants for both oxidative and reductive intracomplex ET decrease by roughly the same factor (Table 3). This equality and viscosity-dependence of the rate constants for intracomplex oxidative and reductive triplet ET,  $^3k_{f,ox} \approx ^3k_{f,red}$ , demonstrates that the measured intracomplex rate constant for charge separation reflects not the ET process itself but rather the rate constant for interconversion among conformations of the bound complex; conformational interconversion on the  $\mu s$ –ms time scale serves as a “gate” to the intracomplex charge separation triplet ET.<sup>27,28</sup>

## SUMMARY

We have shown that photoinitiated electron flow within the  $[MMb:cyt\ b_5]$  complex ( $M = Mg$  or  $Zn$ ) that is stabilized by three D/E  $\rightarrow$  K mutations of Mb can indeed be “symmetrized”; the complex exhibits both oxidative and reductive ET quenching of both the singlet and triplet photoexcited MMb states, with the direction of electron flow being determined by the oxidation state of the cyt  $b_5$  partner,  $Fe^{3+}cyt\ b_5$  or  $Fe^{2+}cyt\ b_5$ . Despite a large disparity in driving force in favor of photooxidation relative to photoreduction ( $\delta(-\Delta G^0) \approx 0.4$  eV,  $M = Mg$ ;  $\approx 0.2$  eV,  $M = Zn$ ), the ultrafast intracomplex reductive and oxidative ET quenchings of  $^1MMb$  surprisingly have the same average ET rate constants of  $^1k_f \approx 10^8 s^{-1}$ . Equally surprising, the intracomplex reductive and oxidative ET quenchings of  $^3MMb$  are again the same within error,  $^3k_f \approx 10^5 s^{-1}$ .

The equality of the rate constants for photooxidation and photoreduction of  $^1MMb$  is explainable on energetic grounds; the driving forces for the two reactions have values symmetrically displaced above and below that of the reorganization energy,  $\lambda$ , and thus equal Franck–Condon factors (FC) within the Marcus equation. The progress curves for both directions of electron flow during ET quenching of  $^1MMb$  are nonexponential and viscosity independent, implying the presence of an ensemble of structures that do not interconvert on the time scale of the measurement.

The rate constants for photooxidation and photoreduction of  $^3MMb$  are again equal despite a large difference in driving force, but in this case the driving force difference predicts a large difference in FC and thus in rate constant. This behavior is

explained by the findings that the progress curves are exponential and the rate constants decrease inversely with viscosity, which indicate that the quenching constants are not ET rate constants at all, but instead that the reactions are gated by intracomplex conformational interconversion. The control of ET on the time scale of triplet-state quenching by conformational interconversion underscores the important point that protein motions can control even intracomplex ET reactions when they occur on the  $\mu s$ –ms time scale, suggesting that reconsideration of numerous such earlier studies might be productive, whereas the independence of the singlet-state ET from such motions indicates that they are not likely to affect the relatively few ET reactions on the ns time scale.

## ASSOCIATED CONTENT

### Supporting Information

Expanded Materials and Methods, determination of driving forces for singlet and triplet electron transfer, difference spectra and kinetic traces for  $[^1ZnMb:cyt\ b_5]$ , Förster resonance energy transfer considerations, and Marcus plot for  $[^1ZnMb:cyt\ b_5]$  complexes. This material is available free of charge via the Internet at <http://pubs.acs.org>.

## AUTHOR INFORMATION

### Corresponding Author

bmh@northwestern.edu

### Notes

The authors declare no competing financial interest.

## ACKNOWLEDGMENTS

N.P.C. and B.M.H. gratefully acknowledge financial support from the National Institute of Health (HL 63203). This work was also supported by the Chemical Sciences, Geosciences, and Biosciences Division, Office of Basic Energy Sciences, DOE under Grant No. DE-FG02-99ER14999 (M.R.W.). R.M.Y. gratefully acknowledges the Camille and Henry Dreyfus Postdoctoral Program in Environmental Chemistry for support. R.M.Y. and A.L.S. were supported as part of the ANSER Center, an Energy Frontier Research Center funded by the U.S. Department of Energy, Office of Science, Office of Basic Energy Sciences, under Award Number DE-SC0001059.

## REFERENCES

- Hickson, R. C.; Rosenkoetter, M. A. *Am. J. Physiol.* **1981**, *241*, C140.
- Hagler, L.; Coppes, R. I., Jr.; Herman, R. H. *J. Biol. Chem.* **1979**, *254*, 6505.
- Liang, Z.-X.; Jiang, M.; Ning, Q.; Hoffman, B. M. *JBIC* **2002**, *7*, 580.
- Trana, E. N.; Nocek, J. M.; Knutson, A. K.; Hoffman, B. M. *Biochemistry* **2012**, *51*, 8542.
- Nocek, J. M.; Knutson, A. K.; Xiong, P.; Co, N. P.; Hoffman, B. M. *J. Am. Chem. Soc.* **2010**, *132*, 6165.
- Xiong, P.; Nocek, J. M.; Vura-Weis, J.; Lockard, J. V.; Wasielewski, M. R.; Hoffman, B. M. *Science* **2010**, *330*, 1075.
- Conklin, K. T.; McLendon, G. *Inorg. Chem.* **1986**, *25*, 4804.

- (8) Cheng, J.; Zhou, J. S.; Kostic, N. M. *Inorg. Chem.* **1994**, *33*, 1600.
- (9) Low, D. W.; Winkler, J. R.; Gray, H. B. *J. Am. Chem. Soc.* **1996**, *118*, 117.
- (10) Hoffman, B. M.; Celis, L. M.; Cull, D. A.; Patel, A. D.; Seifert, J. L.; Wheeler, K. E.; Wang, J.; Yao, J.; Kurnikov, I. V.; Nocek, J. *Proc. Natl. Acad. Sci. U.S.A.* **2005**, *102*, 3564.
- (11) Magner, E.; McLendon, G. *J. Phys. Chem.* **1989**, *93*, 7130.
- (12) Zhou, J. S.; Tran, S. T.; McLendon, G.; Hoffman, B. M. *J. Am. Chem. Soc.* **1997**, *119*, 269.
- (13) Zang, L.-H.; Maki, A. H. *J. Am. Chem. Soc.* **1990**, *112*, 4346.
- (14) Berglund, J.; Pascher, T.; Winkler, J. R.; Gray, H. B. *J. Am. Chem. Soc.* **1997**, *119*, 2464.
- (15) McLendon, G. L.; Winkler, J. R.; Nocera, D. G.; Mauk, M. R.; Mauk, A. G.; Gray, H. B. *J. Am. Chem. Soc.* **1985**, *107*, 739.
- (16) Chibisov, A. K. *Photochem. Photobiol.* **1969**, *10*, 331.
- (17) Carapellucci, P. A.; Mauzerall, D. *Ann. N.Y. Acad. Sci.* **1975**, *244*, 214.
- (18) Shen, C. Y.; Kostic, N. M. *Inorg. Chem.* **1996**, *35*, 2780.
- (19) Jankowska, K. I.; Pagba, C. V.; Chekler, E. L. P.; Deshayes, K.; Piotrowiak, P. *J. Am. Chem. Soc.* **2010**, *132*, 16423.
- (20) Lloyd, E.; Ferrer, J. C.; Funk, W. D.; Mauk, M. R.; Mauk, A. G. *Biochemistry* **1994**, *33*, 11432.
- (21) Funk, W. D.; Lo, T. P.; Mauk, M. R.; Brayer, G. D.; MacGillivray, R. T. A.; Mauk, A. G. *Biochemistry* **1990**, *29*, 5500.
- (22) Wang, Y.-H.; Cui, J.; Sun, Y.-L.; Yao, P.; Zhuang, J.-H.; Xie, Y.; Huang, Z.-X. *J. Electroanal. Chem.* **1997**, *428*, 39.
- (23) Young, R. M.; Dyar, S. M.; Barnes, J. C.; Juricek, M.; Stoddart, J. F.; Co, D. T.; Wasielewski, M. R. *J. Phys. Chem. A* **2013**, *117*, 12438.
- (24) Berberan-Santos, M. N.; Bodunov, E. N.; Valeur, B. *Chem. Phys.* **2005**, *315*, 171.
- (25) Keinan, S.; Nocek, J. M.; Hoffman, B. M.; Beratan, D. N. *Phys. Chem. Chem. Phys.* **2012**, *14*, 13881.
- (26) Given that the driving forces ( $-\Delta G_0$ ) and consequently the expected ET rate constants for the two back reactions (charge recombination) are the same on both the singlet and triplet timescales (Table 1), the accumulations of the charge-separated species are expected to be even smaller on the triplet time scale than on the singlet time scale as the charge recombination processes are expected to be much faster than the preceding triplet ET charge separation processes based on the relative driving forces.
- (27) Hoffman, B. M.; Ratner, M. R. *J. Am. Chem. Soc.* **1987**, *109*, 6237.
- (28) Patel, A. D.; Nocek, J. M.; Hoffman, B. M. *J. Phys. Chem. B* **2008**, *112*, 11827.